The Japan Society of Applied Physics

REGULAR PAPER

Structural and optical analyses of $Al_xGa_{1-x}N$ thin films grown by metal organic chemical vapor deposition

View the article online for updates and enhancements.

Related content

- Buffer optimization for crack-free GaN epitaxial layers grown on Si(1 1 1) substrate by MOCVD
Engin Arslan, Mustafa K Ozturk, Ali Teke et al.

- Structural characterization of Al0.55Ga0.45N epitaxial layer determined by high resolution x-ray diffraction and transmission electron microscopy
Qing-Jun Xu, Bin Liu, Shi-Ying Zhang et al.

- Structural Properties of GaN Films with AlN Buffer Layers with Varying Growth Temperatures by Plasma-Assisted Molecular Beam Epitaxy
Byoung-Rho Shim, Hideyuki Okita, Kulandaivel Jeganathan et al.

Recent citations

- Composition and temperature dependent optical properties of Al x Ga 1-x N alloy by spectroscopic ellipsometry
Yao Liu *et al*

- Influence of TMIn flow rate on structural and optical quality of AlInGaN/GaN epilayers grown by MOCVD
R. Loganathan *et al*

Structural and optical analyses of $Al_xGa_{1−x}N$ thin films grown by metal organic chemical vapor deposition

Bahadir Kucukgok[1], Na Lu[2]*, Ian T. Ferguson[1]*, Shu Chang Wang[3], Xiong Zhang[3], and Zhe Chuan Feng[4]

[1]Department of Electrical and Computer Engineering, University of North Carolina at Charlotte, Charlotte, NC 28223, U.S.A.
[2]Department of Engineering Technology, University of North Carolina at Charlotte, Charlotte, NC 28223, U.S.A.
[3]School of Electronic Science and Engineering, Southeast University, Nanjing 210096, China
[4]Institute of Photonics and Optoelectronics, and Department of Electrical Engineering, National Taiwan University, Taipei 106-17, Taiwan
E-mail: Na.Lu@uncc.edu; ianf@uncc.edu

A series of $Al_xGa_{1−x}N$ thin films with $x = 0.20$–0.60 were grown by metal organic chemical vapor deposition (MOCVD) on sapphire (0001) substrate using AlN buffer layer. High resolution X-ray diffraction (HRXRD) was performed for (0002), (0004), and (0006) reflections to investigate the threading dislocation density in variation with Al composition by X-ray analysis technique; Williamson–Hall (WH) plot. A symmetric high resolution 2θ–ω scans exhibit high crystal quality for all the AlGaN samples. A room temperature deep ultraviolet (DUV) photoluminescence (PL) spectroscopy (excitation at 248 nm) has also been employed to investigate the effect of various Al compositions on crystal structure of the thin film layers. It was observed that the band edge transition peak energy blueshifts from 3.87 eV for $x = 0.23$ to 4.55 eV for $x = 0.47$. In addition to the band edge transition, each spectrum also shows deep impurity transitions. © 2015 The Japan Society of Applied Physics

1. Introduction

The III–V semiconductors of AlN, GaN, and InN and their ternary alloys are recognized as favorable materials for optoelectronic device applications and high-temperature electronic devices due to their tunable bandgap and superior stability at high temperatures.[1–12] For instance, deep ultraviolet (UV) light emitting diodes (LEDs) and laser diodes (LDs) as well as medical devices, water/air purification, and free-space non-line-of-sight communication.[2–4] The growth and doping techniques for III–V semiconductors are more established and reliable as compared II–VI materials, for example, zinc oxide.[13,14] Due to its wide applications, achieving high film quality becomes crucial to the success of all III–V devices. In general, the substrate choice for such semiconductors is mostly sapphire with the hexagonal wurtzite structure. However, these III–V semiconductors thin films typically have high density of structural defects, unlike GaAs or InP[12] such as high defect densities, mosaicity, tilted and twisted small crystallites owing to the large lattice mismatch (∼16%) and the variance in thermal expansion coefficients between substrate and films resulting in large dislocation content up to 10^{10} cm$^{−2}$ likewise residual deterioration.[1,2] To address these issues, a low-temperature AlN or GaN buffer layer has been used but the films still have threading dislocations ∼10^8–10^{10} cm$^{−2}$.[1–3] In addition, inefficient cracking of precursor gas, such as ammonia (NH$_3$), in metal organic chemical vapor deposition (MOCVD) growth process often lead to high dislocation density.[4] These high density defects are detrimental for device applications, for instance, in LEDs the light extraction efficiency significantly decreases due to structural defects. Therefore, it is vital to conduct structural and optical analyses to understand the underlying mechanism of defect structures and improve crystal quality of III–V materials to obtain efficient devices. The defect densities in hexagonal GaN-based materials are usually determined using transmission electron microscopy (TEM); however this method is destructive and sample preparation procedures take a long time.[4–7] In contrast, high-resolution X-ray diffraction (HRXRD) is non-destructive and rapid characterization method for the quality of semiconductor thin films and devices.[1–8] Symmetric X-ray rocking curves (ω-scans) have been broadly performed to study mosaic and thus dislocations in thin films.[5–7]

For the purpose of this study, three MOCVD grown epitaxial hexagonal AlGaN films on sapphire (0001) substrate using AlN buffer layer were examined to understand various Al compositions in the films and their structural and optical properties, including columnar structures, heterogeneous strain, correlation lengths normal and parallel to the substrate surface, tilt and twist, and dislocation densities from HRXRD measurements using X-ray analysis technique; Williamson–Hall (WH) plot. A room temperature deep ultraviolet (DUV) photoluminescence (PL) spectroscopy (excitation at 248 nm) has also been employed to investigate the effect of various Al compositions on crystal structure and bandgap energy of the thin film layers. The results provide insight on $Al_xGa_{1−x}N$ thin films deterioration factors and mechanisms to improve growth conditions for better crystal structures.

2. Experimental methods

The $Al_xGa_{1−x}N$ ($0.23 \leq x \leq 0.60$) epi layers were grown on c-plane sapphire substrates in a low pressure (40 Torr) MOCVD system. Trimethylaluminum (TMA), trimethylgallium (TMG), and NH$_3$ were used as the precursors for Al, Ga, and N, respectively. Prior to the growth, the sapphire substrates were heated to 1100 °C in H$_2$ ambient to remove surface contamination. A 20-nm-thick low-temperature (LT)-grown AlN nucleation layer with a V/III ratio of 3000 was firstly deposited on the sapphire substrate at 600 °C. The temperature was then raised to 1040 °C to grow a high-temperature (HT) AlN interlayer. Finally a 600-nm-thick $Al_xGa_{1−x}N$ epi-layer was grown on HT-AlN interlayer at a growth temperature of 1140 °C. HRXRD measurements were performed using a Philips X'Pert MRD triple-axis diffractometer equipped with a four crystals Ge(220) monochromator in the incident beam optics and a Cu sealed anode. Instrument broadening was neglected in this study. In particular, angular scans (ω scans) (0002), (0004), (0006) and radial scans (2θ–ω scans) (0002), (0004), (0006) in symmetric reflections were performed.
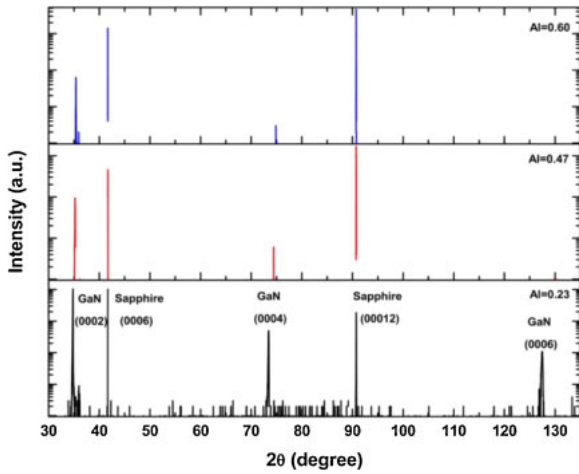
Fig. 1. (Color online) High resolution 2θ–ω scans for a set of Al-content (0.20–0.60) $Al_xGa_{1-x}N$ thin films with ranging from 30 to 130°.

The mosaic structure of the thin layers is evaluated by the size and the angular distribution of the mosaic blocks[7] by using WH plots. Four parameters; lateral coherence length ($L_{||}$), vertical coherence length ($L_{\perp}$), twist (α_{twist}), and tilt (α_{tilt}) have been used to characterize the mosaicity. The tilt and twist angles provide information about the angular distribution of the crystallographic direction of the mosaic blocks perpendicular and vertical to the substrate plane, and the lateral and vertical coherence lengths are attributed to the mosaic block size. By using WH technique, the broadening of the rocking curve (ω scans) scans are influenced only by the tilt and the coherence length parallel to the reflection substrate. Likewise, in the triple-axis 2θ–ω scans the coherence length normal to the substrate surface and the heterogeneous strain ($\varepsilon_{\perp}$) along the c-axis result in the profile broadening.[7,8,12] By performing WH plot analyze, we can evaluate the vertical coherence length, and heterogeneous strain along the c-axis. Moreover, DUV PL spectroscopy was conducted at room temperature. The excitation source was 248 nm, NeCu continuous wave laser.

3. Results and discussion

3.1 Results

A symmetric high resolution 2θ–ω scans exhibit high crystal quality for all the $Al_xGa_{1-x}N$ samples is shown in Fig. 1. The intensity of 2θ–ω scan of (0002) is less sensitive for the variation in unit cell parameters, which is induced by composition and strain differences.[9] The composition of $Al_xGa_{1-x}N$ layers were conducted from 2θ–ω scans of the (0002) reflection based on a relationship between the lattice parameter and the chemical composition, assuming the validity of Vegard's law.[15] In order to investigate the effects of different Al compositions (0.23, 0.47, and 0.60) on the structural properties of AlGaN layers, WH plots have been used to extract values for $L_{||}$, α_{tilt}, N_{screw}, $L_{\perp}$, and $\varepsilon_{\perp}$. Figure 2(a) shows the WH plots used to obtain the $L_{||}$ and α_{tilt} which are the dominant parameters in calculating screw dislocation density. The Burgers vector of c-axis for AlGaN thin films are determined as $|b_c| = 5.185$ Å for calculating screw dislocation density. Figure 2(b) is used to determine the physical sizes of the columnar structure, $L_{\perp}$ and strain

(a)

(b)
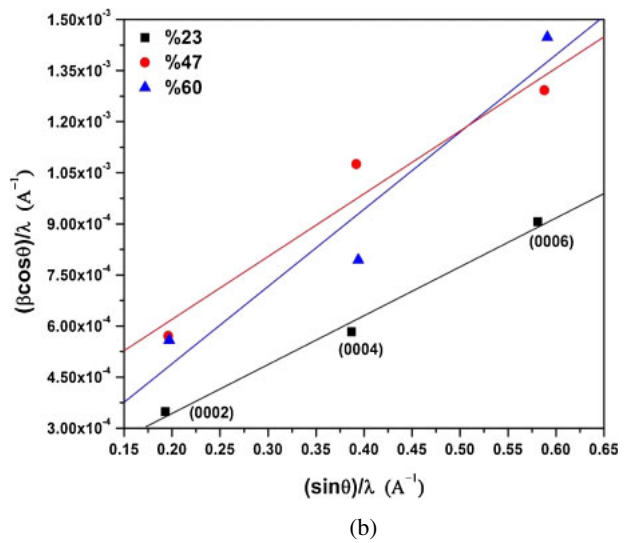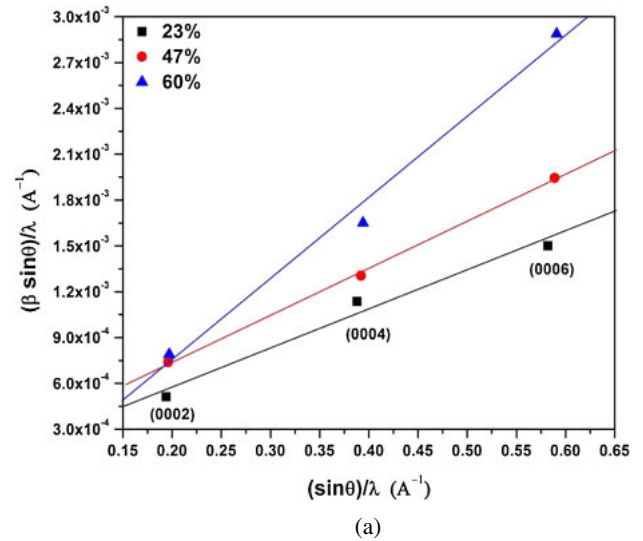
Fig. 2. (Color online) Williamson–Hall plots for $Al_xGa_{1-x}N$ thin films. (a) The y-intersect (Y_0) of the fitted line is used to calculate the lateral coherence length using $L_{||} = 0.9/2Y_0$ where β_ω, θ, and λ are the integral width of the measured profile, Bragg reflection angle, X-ray wavelength (0.15406 nm), respectively. The slope of the fitted line is the tilt angle and is used to evaluate the screw dislocation with the Burgers vector $|b_c|N_{screw} = \alpha_{tilt}^2/4.35|b_c|^2$ (b) the line slope provides the information of the heterogeneous strain along the c-axis as $\beta_{2\theta-\omega}(\cos\theta)/\lambda$ is plotted against $(\sin\theta)/\lambda$ for each reflection, and fitted linearly, with using y intersection value.

component, $\varepsilon_{\perp}$. One can see the influence of Al compositions on screw dislocation density, tilt angle, c lattice constant and heterogonous strain parallel to c lattice in Figs. 3(a) and 3(b). The lattice constant c was obtained by HRXRD measurements with using the lattice spacing d_{002} obtained via Eqs. (1) and (2):[10]

$$2d_{002}\sin(\theta_{002}) = \lambda, \tag{1}$$

$$\frac{1}{d_{hkl}^2} = \frac{4(h^2 + hk + k^2)}{3a^2} + \frac{l^2}{c^2}. \tag{2}$$

Table I depicts the summary of the mosaic structure factors of AlGaN samples measured from HRXRD. Moreover, Fig. 4 exhibits the room temperature PL spectrum of $Al_xGa_{1-x}N$ samples and one can observe that the band edge transition peak energy blueshifts from 3.87 eV for $x = 0.23$ to

(a)
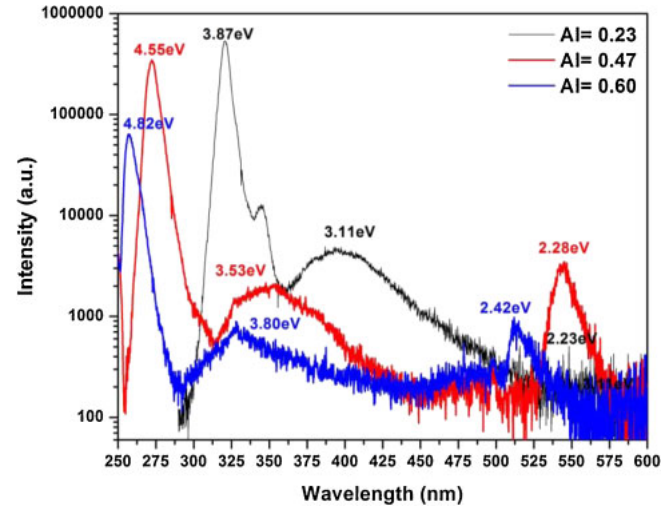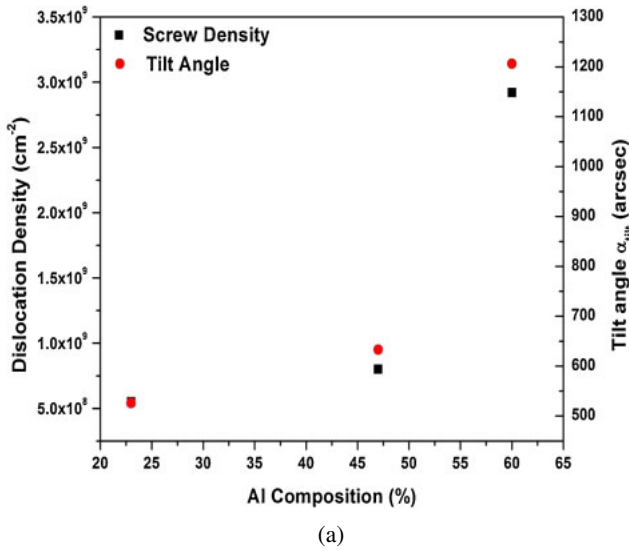
Fig. 4. (Color online) PL spectrum under DUV 248 nm excitation of $Al_xGa_{1-x}N$ thin films with Al-content (0.20 and 0.47).

(b)
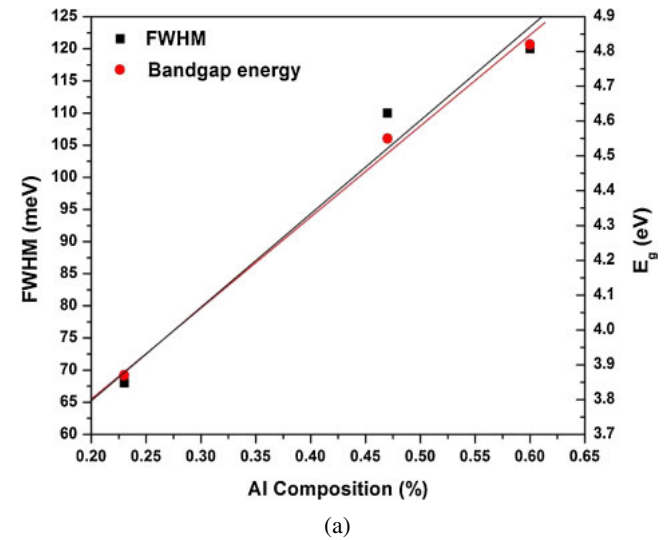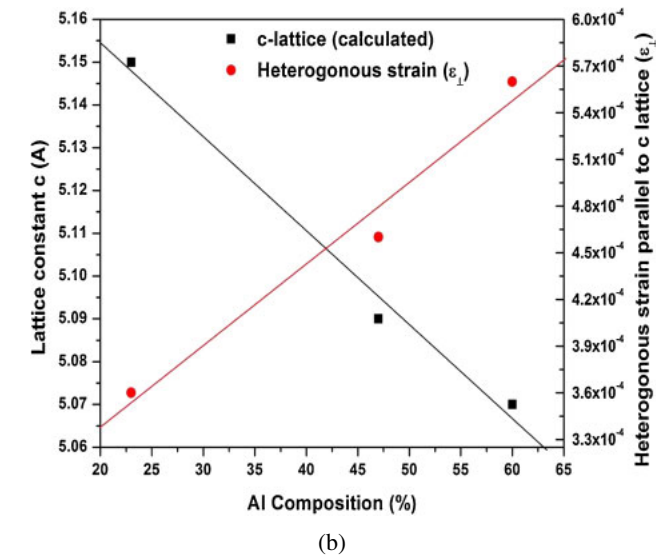
Fig. 3. (Color online) Variations of (a) dislocation density and tilt angle and (b) lattice constant c and heterogonous strain with respect to Al compositions, respectively. The straight lines are guided to the eye.

(a)

Table I. Analysis summary of HRXRD measurements of $Al_xGa_{1-x}N$ thin films.

	$Al_{0.23}Ga_{0.77}N$	$Al_{0.47}Ga_{0.53}N$	$Al_{0.60}Ga_{0.40}N$
Lateral coherence length $L_{\parallel}$ (μm)	0.74	0.36	NA
Vertical coherence length $L_{\perp}$ (μm)	0.79	0.17	1.02
Tilt angle α_{tilt} (arcsec)	526	633	1206
Screw dislocation N_{screw} (cm^{-2})	0.55×10^9	0.80×10^9	2.92×10^9
Heterogonous strain parallel to c lattice ($\varepsilon_{\perp}$)	3.6×10^{-4}	4.6×10^{-4}	5.6×10^{-4}

(b)

Fig. 5. (Color online) Variation of (a) FWHM and energy bandgap and (b) PL spectra peak position (E_{imp}) of deep impurity transition with respect to Al compositions. The straight lines are guided to the eye.

4.55 eV for $x = 0.47$. In addition to the band edge transition, each spectrum also shows deep impurity transitions. We have also investigated the effective band gap position as well as its full width half maximum (FWHM) value and the energy position of the impurity transition seen in Fig. 4 with respect to Al composition in Figs. 5(a) and 5(b).

3.2 Discussion

From Fig. 2(a), we estimate the tilts for three AlGaN samples to be, respectively, 526, 622, and 1206 arcsec. This can be interpreted to a screw dislocation density of 0.55×10^9, 0.80×10^9, and $2.92 \times 10^9 \, cm^{-2}$, respectively. The corresponding lateral coherence lengths for these samples are estimated to be 0.74 and 0.36 μm for $Al_{0.23}Ga_{0.77}N$ and $Al_{0.47}Ga_{0.53}N$ samples, respectively. These results show that the AlGaN layer grown on AlN buffer layer improves the mosaicity compared to AlGaN layer grown on sapphire without the buffer layer. Although, high temperature grown AlGaN layer has improved quality, it naturally replicates with the considerable mosaic structure of the LT-grown AlN buffer.[11] The vertical coherence lengths and heterogonous strain parallel to c lattice are evaluated in Fig. 2(b). The corresponding lateral coherence lengths for these samples are estimated to be 0.79, 0.17, and 1.02 μm respectively. In addition, the heterogeneous strains in the three samples are found 3.6×10^{-4}, 4.6×10^{-4}, and 5.6×10^{-4}, respectively. The reason of the heterogeneous strain could be the misfit dislocations with $b_E = 1/3\langle 11\bar{2}0\rangle$ existent in the film–sapphire interface region.[11,12] Figure 3(a) indicates that the screw dislocation density and tilt angle increase with Al composition and shows similar trend. This is because both these physical parameters are directly proportional with each other through screw dislocation formula shown in Fig. 2(a) caption. Furthermore, this behavior could also be explained by the unit cell parameters' origin of the GaN and AlN.[7] AlN has lattice parameters ($a = 3.112$ Å, $c = 4.981$ Å) smaller than that of GaN ($a = 3.189$ Å, $c = 5.185$ Å).[15] Thus the lateral coherence length of the AlGaN columnar structures with higher Al composition could be degraded more compared to the one with lower Al composition. Figure 3(b) illustrates the well-known phenomenon that is the lattice parameters of the alloy films are influenced by strain and composition. As Al composition increases lattice constant c decreases while heterogeneous strain parallel to c lattice increases. Therefore, amount of aluminum affects the geometric size of columnar structure with an effect on the strain component and results in crystalline defects induced by lattice strain/stress and threading dislocations in the layers. As a consequence, the material is assumed to be fully strained or a relaxed. For further analyses, reciprocal space mapping (RSM) would be performed for each sample. Table I shows mean geometric size of columnar structures as well as dislocation density for the epitaxial AlGaN layers. In Table I, one value is not reported as a result of weak HRXRD intensity and thus large error on the sample.

Moreover, one can see from Fig. 4 that the compositional dependence of bandgap energy of AlGaN layers with deep impurity transitions. As the Al composition enhances the band edge transition peak energy blueshifts from 3.87 eV for $x = 0.23$ to 4.82 eV for $x = 0.60$ in $Al_xGa_{1-x}N$ alloys that can be seen in Fig. 5(a) as well. This is due to the phenomenological quadratic dependence on the Al composition, as given by[16–18]

$$E_g(Al_xGa_{1-x}N) = xE_g(AlN) + (1-x)E_g(GaN) \\ - bx(1-x), \qquad (3)$$

where x and b are the Al composition and bowing parameter, respectively. As is well known, band-edge shifts are strain-related; hence Fig. 4 is also confirming the strain relaxation of the crystal structures of AlGaN layers. We also approximated compositional dependence of the energy bandgap of $Al_xGa_{1-x}N$ by using Eq. (3). Energy band gaps of 6.05 and 3.43 eV[18] for AlN and GaN and b value of 1[19] were used, respectively. The energy bandgap of AlGaN samples were found 3.85, 4.41, and 4.76 eV, respectively. It can be clearly realized that the difference between the measured and calculated energy bandgap values are due to the uncertainty of b parameter since it is critical to measure energy bandgap over a large range of composition to achieve accurate calculation of b. In addition, strain and composition fluctuation can also have impact on the measured bowing parameters in the literature.[16–18]

In addition to the band edge transition, each spectrum also depicts deep impurity transitions. For instance, the impurity emission peak of nearby 2.15 eV was induced by the transition from a shallow donor to deep acceptor, which correlates with yellow luminescence (YL) in GaN.[20–22] Recent studies show that the deep acceptor involved in the YL is correlated with V_{Ga} composed of two negative charges called $(V_{III}$ complex$)^{2-}$ such as $(V_{Ga}-O_N)^{2-}$ or $(V_{Ga}-Si_{Ga})^{2-}$.[22–24] Based on study of Nepal et al. and his colleagues, impurity transitions with emission energies larger than $(V_{III})^{3-}$ and $(V_{III}$ complex$)^{2-}$ connected transitions has been observed in Fig. 5(b). It can be seen that the energy position of the impurity transition increases with Al concentration and has the same trend with $(V_{III})^{3-}$ and $(V_{III}$ complex$)^{2-}$. Therefore, it might be suggested that these impurity transitions that was observed in Fig. 4 are of the same physical origin and donor–acceptor pair (DAP) connecting with shallow donors and deep acceptors.

4. Conclusions

In this work, we have studied the threading dislocation density in variation with Al composition by X-ray analysis technique; WH plot with a series of AlGaN thin films with $x(Al) = 0.20$–0.60, which were grown by metal organic chemical vapor deposition (MOCVD) on sapphire (0001) substrate using AlN buffer layer. WH plots have shown that AlGaN samples have larger tilt angles and screw dislocation densities, and smaller lateral coherence length as the Al composition increases. The lattice stress/strain of AlGaN with different Al contents has also been analyzed. Room temperature PL studies and impurity transition levels have also investigated for $Al_xGa_{1-x}N$ alloys.

1) V. P. Kladko, A. F. Kolomys, M. V. Slobodian, V. V. Strelchuk, V. G. Raycheva, A. E. Belyaev, S. S. Bukalov, H. Hardtdegen, V. A. Sydoruk, N. Klein, and S. A. Vitusevich, J. Appl. Phys. **105**, 063515 (2009).
2) B. Heying, X. U. Wu, S. Keller, Y. Li, D. Kapolnek, B. P. Keller, S. P. DenBaars, and J. S. Speck, Appl. Phys. Lett. **68**, 643 (1996).
3) T. L. Song, S. J. Chua, E. A. Fitzgerald, P. Chen, and S. Tripathy, Appl. Phys. Lett. **83**, 1545 (2003).

4) T. D. Moustakas, Y. Liao, C. Kao, C. Thomidis, A. Bhattacharyya, D. Bhattarai, and A. Moldawer, Proc. SPIE **8278**, 82780L (2012).
5) N. A. Mahadik, S. B. Qadri, and M. V. Rao, Appl. Phys. Lett. **93**, 222106 (2008).
6) F. Meng, J. Zhang, H. Zhou, J. Ma, J. Xue, L. Dang, L. Zhang, M. Lu, S. Ai, X. Li, and Y. Hao, J. Appl. Phys. **112**, 023707 (2012).
7) H. Kang, S. Kandoor, S. Gupta, I. Ferguson, S. P. Guo, and M. Pophristic, Phys. Status Solidi C **2**, 2145 (2005).
8) J.-Q. Liu, Y.-X. Qiu, J.-F. Wang, K. Xu, and H. Yang, Chin. Phys. Lett. **28**, 016101 (2011).
9) M. Jayasakthi, R. Ramesh, P. Arivazhagan, R. Loganathan, K. Prabakaran, M. Balaji, and K. Baskar, J. Cryst. Growth **401**, 527 (2014).
10) H. F. Liu, S. B. Dolmanan, L. Zhang, S. J. Chua, D. Z. Chi, M. Heuken, and S. Tripathy, J. Appl. Phys. **113**, 023510 (2013).
11) H.-M. Wang, J.-P. Zhang, C.-Q. Chen, Q. Fareed, J.-W. Yang, and M. Asif Khan, Appl. Phys. Lett. **81**, 604 (2002).
12) T. Metzger, R. Höpler, E. Born, O. Ambacher, M. Stutzmann, R. Stömmer, M. Schuster, H. Göbel, S. Christiansen, M. Albrecht, and H. P. Strunk, Philos. Mag. A **77**, 1013 (1998).
13) B. Hussain, B. Kucukgok, M. Y. A. Raja, B. Klein, N. Lu, and I. T. Ferguson, Proc. SPIE **8987**, 898718 (2014).
14) S. C. Jain, M. Willander, J. Narayan, and R. Van Overstraeten, J. Appl. Phys. **87**, 965 (2000).
15) M. A. Moram and M. E. Vickers, Rep. Prog. Phys. **72**, 036502 (2009).
16) J. Wu, J. Appl. Phys. **106**, 011101 (2009).
17) M. Androulidaki, N. T. Pelekanos, K. Tsagaraki, E. Dimakis, E. Iliopoulos, A. Adikimenakis, E. Bellet-Amalric, D. Jalabert, and A. Georgakilas, Phys. Status Solidi C **3**, 1866 (2006).
18) H. X. Jiang and J. Y. Lin, Opto-Electron. Rev. **10**, 271 (2002).
19) D. Brunner, H. Angerer, E. Bustarret, F. Freudenberg, R. Hopler, R. Dimitrov, O. Ambacher, and M. Stutzmann, J. Appl. Phys. **82**, 5090 (1997).
20) T. Mattila and R. M. Nieminen, Phys. Rev. B **55**, 9571 (1997).
21) J. Neugebauer and C. G. Van de Walle, Appl. Phys. Lett. **69**, 503 (1996).
22) N. Nepal, M. L. Nakarmi, J. Y. Lin, and H. X. Jiang, Appl. Phys. Lett. **89**, 092107 (2006).
23) I. Gorczyca, N. E. Christensen, and A. Svane, Phys. Rev. B **66**, 075210 (2002).
24) K. B. Nam, M. L. Nakarmi, J. Y. Lin, and H. X. Jiang, Appl. Phys. Lett. **86**, 222108 (2005).